Implementation and performance of the frequency-dependent *GW* method within the PAW framework

M. Shishkin and G. Kresse
Institut für Materialphysik and Centre for Computational Materials Science, Universität Wien, A 1090 Wien, Austria
(Received 14 February 2006; revised manuscript received 28 April 2006; published 6 July 2006)

Algorithmic details and results of fully frequency-dependent G_0W_0 calculations are presented. The implementation relies on the spectral representation of the involved matrices and their Hilbert or Kramers-Kronig transforms to obtain the polarizability and self-energy matrices at each frequency. Using this approach, the computational time for the calculation of polarizability matrices and quasiparticle energies is twice as that for a single frequency, plus Hilbert transforms. In addition, the implementation relies on the PAW method, which allows to treat *d*-states with relatively modest effort and permits the reevaluation of the core-valence interaction on the level of the Hartree-Fock approximation. Tests performed on an *sp* material (Si) and materials with *d* electrons (GaAs and CdS) yield quasiparticle energies that are very close to previous all-electron pseudopotential and all-electron full-potential linear muffin-tin-orbital calculations.

DOI: 10.1103/PhysRevB.74.035101 PACS number(s): 71.10.−w, 71.15.Mb, 71.20.Nr

I. INTRODUCTION

The accurate calculation of excitation spectra (i.e., quasiparticle energies) is a long-standing problem in solid state physics, as these can be directly compared to electronic and optical measurements such as electron photoemission, photoabsorption, photoluminescence, etc. The widely used density functional theory (DFT) performs reasonably well for the determination of structural properties of many materials but fails to predict the band gaps and sometimes even general characteristics of the conduction band. Such a failure of the DFT is not unexpected, since there exists no formal justification to interpret the DFT eigenvalues as quasiparticle (QP) energies. As a remedy to this inherent problem, the *GW* approximation is widely used, which generally yields significantly better values for quasiparticle energies.[1,2] The predictive capabilities of the *GW* approximation stem from inclusion of many-body effects in the electron-electron interaction and going beyond the mean-field approximation of independent particles.[3] This is achieved via screening the exchange interaction operator with the inverse frequency-dependent dielectric matrix to include many-body interactions between the electrons as opposed to effective local exchange-correlation potentials in DFT.

The downside of such an involved approach, however, is its large computational cost, caused by the evaluation of dielectric matrices, their inversion, and solving a non-Hermitian nonlinear eigenvalue problem. Therefore, *GW* calculations are usually restricted to small systems. To reduce the computational effort, the *GW* method relied initially on a simplified inclusion of dynamical effects (frequency dependence) via the plasmon-pole model.[4–6] Although in this case only the static dielectric matrix is calculated explicitly, the plasmon-pole model proved to perform reasonably well at least for *sp* materials. However, the method is principally limited to the calculation of quasiparticle energies and does not permit the evaluation of other useful quantities such as quasiparticle lifetimes or spectral functions. Moreover, for materials with *d* electrons, the reliability of the plasmon-pole model is disputable.[1] Therefore, even in some early implementations of the *GW* method, dielectric matrices have been calculated precisely at each frequency.[7]

To circumvent the slow performance of the *GW* method, the space-time method, which resorts to imaginary time and frequency,[8–10] has been suggested. The only drawback of this method is that it requires an analytical continuation from the imaginary axis to the real axis. More recently, Miyake *et al.*[11] proposed an efficient method that avoids an explicit calculation of the real part of the polarizability matrix at each frequency by a spectral representation of the polarizability and a subsequent Hilbert or Kramers-Kronig transform to obtain the full polarizability at a frequency grid. In the present implementation, we adopt a similar strategy and extend it to the calculation of quasiparticle energies.

A further problem is posed by *d* and *f* electrons, especially, if a plane wave basis set is used in combination with pseudopotentials. Quite a large number of plane waves are required for a reasonable description of these localized states, which significantly slows *GW* calculations. To circumvent this problem, Gaussian orbitals or localized basis sets can be applied.[12–15] This was first done in the linear muffin-tin-orbital (LMTO) method,[12] which has the drawback of a poor description of the interstitial region and an *a priori* constraint on the form of the electronic charge distribution. More elaborate full-potential linear muffin-tin-orbital (FP-LMTO) or full-potential linear augmented plane-wave (FLAPW) methods, which utilize the localized basis set in the muffin-tin region and plane waves in the interstitial region, have been used in combination with *GW* for a precise and unbiased treatment of the response functions. Representing the polarizability in the spheres and the interstitial region with high accuracy is, however, cumbersome and difficult, as well as computationally demanding.[17,18] A very promising alternative is the PAW method,[19] first adopted by Arnaud and co-workers for the *GW* case.[20,21] A simplified PAW *GW* scheme that uses a model dielectric function together with a plasmon-pole approximation for the dynamical contribution has also been implemented in the VASP code.[22] The PAW method has three major advantages. From the FLAPW method it inherits a fast convergence with respect to the basis

set size and, therefore, can be applied efficiently to d and f elements. On the other hand, it is a full potential method with no shape approximation on the charge distribution, allowing in principle for exact results within the considered theoretical framework. Compared to other full potential methods, it, however, retains most of the simplicity of a pseudopotential approach. Section II A will convey why this method is particularly well suited for an implementation of the *GW* method.

In this paper we discuss the implementation of the *GW* approximation in the PAW code VASP and carefully evaluate important aspects of the method. In Sec. II we give the expressions for the relevant quantities in the PAW formalism (polarizabilities, dielectric matrices, self-energies, etc.). Section III describes the calculational procedure using spectral representations of frequency-dependent quantities. We use a method similar to the one proposed in Ref. 10, however, the spectral representations and Hilbert transforms are used not only to calculate the polarizabilities but also to determine the self-energies at all required frequencies. Results of our calculations are provided in Sec. IV. We put particular emphasis on understanding the discrepancy between published pseudopotential and all-electron data. In order to disentangle these discrepancies, *GW* calculations are performed using various PAW potentials, and high lying core shells are successively unfrozen. Furthermore, we treat the core-valence interaction either in DFT or using the Hartree-Fock approximation. As test cases, we consider Si and materials that include d electrons (GaAs, CdS). The conclusions are given in Sec. V.

II. *GW* METHOD

A. Basics of the PAW method

The basic concepts of the PAW method that are necessary to understand the present *GW* implementation have been outlined in Refs. 29 and 30. More extensive descriptions can be found in Ref. 19 (the present notation closely follows Ref. 31). Here we give a simple intuitive account of the PAW method.

The important concept of the PAW method is that of additive augmentation. On the plane-wave grid, the Hamiltonian is represented in a pseudopotential-like manner, with the only complication that the pseudo-wave-functions are not correctly normalized. To correct for the resultant error, local compensation charges are added in the vicinity of each atom in such a way that the final charge density distribution has, around each atom, exactly the same moments and multipoles as the exact all-electron (AE) charge density. The electrostatic potential determined from this charge distribution is essentially exact in the interstitial region, but the kinetic energy and the potentials are not accurately represented inside the atomic spheres. To make up for the error, the pseudo-wave-functions and AE wave functions are reconstructed inside the PAW spheres, and the resultant energy terms are subtracted and added from the energy (see Fig. 1).

Inside the spheres, the Hamiltonian is equivalent to the usual Kohn-Sham (or *GW*) Hamiltonian using a local basis set. The basis functions used to represent the pseudo and AE wave functions are usually imported from an atomic pseudo-

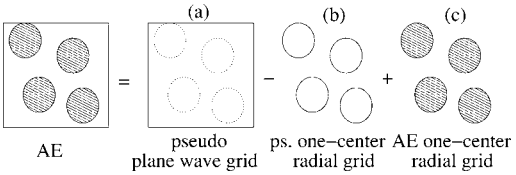

FIG. 1. Illustration of additive augmentation in the PAW method. Pseudized quantities are defined in the entire space on a regular (plane wave) grid (a). To obtain AE energies, the pseudo-wave-functions are reconstructed inside spheres and the corresponding one-center energy terms are subtracted (b), and finally the AE wave functions are reconstructed as well and the AE one-center energies are added (c).

potential generation code and are termed "partial waves." The one-center density matrices (occupancy matrices in the basis spanned by the partial waves) are, however, not free to vary but depend on the wave-function coefficients on the plane-wave grid.

For the implementation of the *GW* method, it is important to emphasize that usually most of the physics is already correctly captured on the plane-wave grid, with the quality of this description matching that of a norm-conserving pseudopotential. The rapid variations of the AE wave functions are however only accounted for on the radial grid. For our *GW* implementation, we have thus decided to implement the plane-wave terms exactly, but to use a simple and physically transparent approximation for the one-center terms (see Sec. II E). Note that it would be possible to add a more sophisticated treatment in the atomic spheres at a later point. This could for instance even include a full quantum chemical description such as configuration interaction (CI).

B. Quasiparticle equations

The quasiparticle energies ($E_{n\mathbf{k}}^{\mathrm{QP}}$) can be calculated, in principle exactly, by searching the roots of the following nonlinear system of equations:

$$(T + V_{n\text{-}e} + V_H - E_{n\mathbf{k}}^{\mathrm{QP}})\psi_{n\mathbf{k}}(\mathbf{r}) + \int d^3\mathbf{r}'\Sigma(\mathbf{r},\mathbf{r}',E_{n\mathbf{k}}^{\mathrm{QP}})\psi_{n\mathbf{k}}(\mathbf{r}'). \tag{1}$$

Here T is the kinetic energy operator, $V_{n\text{-}e}$ is the operator that accounts for the nuclear-electron interactions, V_H is the Hartree potential, and Σ is the self-energy operator, which has the form

$$\Sigma(\mathbf{r},\mathbf{r}',\omega) = \frac{i}{4\pi}\int_{-\infty}^{\infty} e^{i\omega'\delta}G(\mathbf{r},\mathbf{r}',\omega+\omega')W(\mathbf{r},\mathbf{r}',\omega')d\omega' \tag{2}$$

within the *GW* approximation, where G is the Green's function, W is the screened Coulomb interaction, and δ is a positive infinitesimal. The screened interaction W is usually constructed using the polarizability in the random phase approximation (RPA), i.e., excluding vertex corrections. Attempts of inclusion of vertex corrections made in the past resulted only in minor changes of the calculated values (e.g.,

0.05 eV for Si).[24–26] Fully self-consistent calculations, on the other hand, deteriorate the quasiparticle spectrum and yield overestimated gaps.[27,28] In the non-self-consistent GW approximation (G_0W_0), adopted throughout this work, G_0 and W_0 are calculated using LDA Kohn-Sham eigenvalues and eigenfunctions. By approximating the eigenstates of the quasiparticle Hamiltonian [Eq. (1)] by LDA wave functions as well, the eigenvalues can be calculated to first order from the diagonal matrix elements of the QP equation[4]

$$E_{n\mathbf{k}}^{\mathrm{QP}} = \mathrm{Re}[\langle\psi_{n\mathbf{k}}|T + V_{n\text{-}e} + V_H + \Sigma(E_{n\mathbf{k}}^{\mathrm{QP}})|\psi_{n\mathbf{k}}\rangle]. \tag{3}$$

Since Eq. (3) already requires the value of $E_{n\mathbf{k}}^{\mathrm{QP}}$, the equation must be solved by iteration. Using the usual Newton-Raphson method for root finding, one obtains the following update equations:

$$E_{n\mathbf{k}}^{\mathrm{QP}} \leftarrow E_{n\mathbf{k}}^{\mathrm{QP}} + Z_{n\mathbf{k}}\mathrm{Re}[\langle\psi_{n\mathbf{k}}|T + V_{n\text{-}e} + V_H + \Sigma(E_{n\mathbf{k}}^{\mathrm{QP}})|\psi_{n\mathbf{k}}\rangle - E_{n\mathbf{k}}^{\mathrm{QP}}], \tag{4}$$

where Z, the normalization factor, is calculated as

$$Z_{n\mathbf{k}} = \left(1 - \mathrm{Re}\langle\psi_{n\mathbf{k}}|\ \frac{\partial}{\partial\omega}\Sigma(\omega)\Big|_{E_{n\mathbf{k}}^{\mathrm{QP}}}|\psi_{n\mathbf{k}}\rangle\right)^{-1}. \tag{5}$$

The iteration is usually started from the DFT eigenvalues $\epsilon_{n\mathbf{k}}$. All QP energies presented in this work have been calculated using this approach and a *single* iteration, i.e., Eq. (4) was iterated once starting from $E_{n\mathbf{k}}^{\mathrm{QP}} = \epsilon_{n\mathbf{k}}$ on the right-hand side. This is in the spirit of first-order perturbation theory, and hence a well-founded approximation.

C. Evaluation of dielectric matrix

The dynamically screened Coulomb interaction is evaluated by multiplying the bare Coulomb kernel with the inverse dielectric matrix:

$$W_{\mathbf{q}}(\mathbf{G},\mathbf{G}',\omega) = 4\pi e^2 \frac{1}{|\mathbf{q}+\mathbf{G}|}\epsilon_{\mathbf{q}}^{-1}(\mathbf{G},\mathbf{G}',\omega)\frac{1}{|\mathbf{q}+\mathbf{G}'|}. \tag{6}$$

In the RPA the symmetric dielectric matrix is calculated as

$$\epsilon_{\mathbf{q}}(\mathbf{G},\mathbf{G}',\omega) = \delta_{\mathbf{G},\mathbf{G}'} - \frac{4\pi e^2}{|\mathbf{q}+\mathbf{G}||\mathbf{q}+\mathbf{G}'|}\chi_{\mathbf{q}}^0(\mathbf{G},\mathbf{G}',\omega), \tag{7}$$

where $\chi_{\mathbf{q}}^0(\mathbf{G},\mathbf{G}',\omega)$ is the time ordered independent particle polarizability,[32]

$$\chi_{\mathbf{q}}^0(\mathbf{G},\mathbf{G}',\omega) = \frac{1}{\Omega}\sum_{nn'\mathbf{k}} 2w_{\mathbf{k}}(f_{n'\mathbf{k}-\mathbf{q}} - f_{n\mathbf{k}}) \times \frac{\langle\psi_{n'\mathbf{k}-\mathbf{q}}|e^{-i(\mathbf{q}+\mathbf{G})\mathbf{r}}|\psi_{n\mathbf{k}}\rangle\langle\psi_{n\mathbf{k}}|e^{i(\mathbf{q}+\mathbf{G}')\mathbf{r}'}|\psi_{n'\mathbf{k}-\mathbf{q}}\rangle}{\omega + \epsilon_{n'\mathbf{k}-\mathbf{q}} - \epsilon_{n\mathbf{k}} + i\eta\,\mathrm{sgn}[\epsilon_{n'\mathbf{k}-\mathbf{q}} - \epsilon_{n\mathbf{k}}]}. \tag{8}$$

In the last expression, $w_{\mathbf{k}}$ is the k-point weight, $f_{n'\mathbf{k}-\mathbf{q}}$ and $f_{n\mathbf{k}}$ are the one electron occupancies of the corresponding states, $\mathbf{q}$ is a Bloch wave vector, and η is an infinitesimal complex shift. Within the current implementation the quantity $\langle\psi_{n'\mathbf{k}-\mathbf{q}}|e^{-i(\mathbf{q}+\mathbf{G})\mathbf{r}}|\psi_{n\mathbf{k}}\rangle$ (the exchange charge density) is approximated as

$$\langle\psi_{n'\mathbf{k}-\mathbf{q}}|e^{-i(\mathbf{q}+\mathbf{G})\mathbf{r}}|\psi_{n\mathbf{k}}\rangle \approx \langle\tilde{u}_{n'\mathbf{k}-\mathbf{q}}|e^{-i\mathbf{G}\mathbf{r}}|\tilde{u}_{n\mathbf{k}}\rangle + \sum_{ij,R,LM}\langle\tilde{u}_{n'\mathbf{k}-\mathbf{q}}|p_{i\mathbf{k}-\mathbf{q}}\rangle\langle p_{j\mathbf{k}}|\tilde{u}_{n\mathbf{k}}\rangle \times \int d^3r(e^{-i\mathbf{q}(\mathbf{r}-\mathbf{R}_i)}\hat{Q}_{ij}^{LM}(\mathbf{r}-\mathbf{R}_i)e^{-i\mathbf{G}\mathbf{r}}), \tag{9}$$

where $\tilde{u}_{n\mathbf{k}}$ is the cell periodic part of the one-electron pseudo-wave-function $|\tilde{\psi}_{n\mathbf{k}}\rangle = e^{i\mathbf{k}\mathbf{r}}|\tilde{u}_{n\mathbf{k}}\rangle$; $p_{i\mathbf{k}}$ is the $\mathbf{k}$-dependent projector function, related to the usual PAW projector function p_i, centered on the atom with coordinates $\mathbf{R}_i$, through $|p_{i\mathbf{k}}\rangle = e^{-i\mathbf{k}(\mathbf{r}-\mathbf{R}_i)}|p_i\rangle$, and $\hat{Q}_{ij}^{LM}(\mathbf{r}-\mathbf{R}_i)$ are the multipole expansions of the compensation charges (for details we refer to Refs. 29 and 30). The second term is added to restore the correct multipoles of the AE charge density on the plane wave grid ($\tilde{u}_{n\mathbf{k}}$ is not correctly normalized, see Sec. II A). Expression (9) includes only the plane-wave part of the charge distribution and neglects the one-center terms in the PAW spheres, which should be added to reconstruct the all-electron charge density [see Figs. 1(b) and 1(c)]. In the calculation of the dielectric matrix, this approximation can be justified by the observation that the difference between the all-electron and pseudo-charge-density is most pronounced in the short wave range (large $\mathbf{G}$ and $\mathbf{G}'$) and therefore can be usually neglected due to the factor $1/(\mathbf{q}+\mathbf{G})(\mathbf{q}+\mathbf{G}')$ in Eq. (7). Indeed, we found this conjecture confirmed in a recent work on the dielectric properties of simple semiconductors. We find that the inclusion of one-center terms changes the macroscopic dielectric constants by at most 0.3%, even in difficult cases such as GaAs where strongly localized d electrons have to be taken into account.[29] Special care is required for the case $\mathbf{q}=0$. An obvious singularity in the calculation of the dielectric matrix [Eq. (7)] occurs if $\mathbf{G}=0$ or $\mathbf{G}'=0$ (the wings) or $\mathbf{G}=\mathbf{G}'=0$ (the head of the dielectric matrix). Solutions for this specific case have been presented in a recent presentation,[29] which describes the PAW expressions for the head and wings of the dielectric matrix.

D. Self-energy calculation

In the present implementation, the diagonal matrix elements of the self-energy $\Sigma(\omega)_{n\mathbf{k},n\mathbf{k}}$ are calculated as

$$\bar{\Sigma}(\omega)_{n\mathbf{k},n\mathbf{k}} = \frac{1}{\Omega}\sum_{\mathbf{q}\mathbf{G}\mathbf{G}'}\sum_{n'}\frac{i}{2\pi}\int_0^\infty d\omega'\,\bar{W}_{\mathbf{q}}(\mathbf{G},\mathbf{G}',\omega') \times\langle\psi_{n\mathbf{k}}|e^{i(\mathbf{q}+\mathbf{G})\mathbf{r}}|\psi_{n'\mathbf{k}-\mathbf{q}}\rangle\langle\psi_{n'\mathbf{k}-\mathbf{q}}|e^{-i(\mathbf{q}+\mathbf{G}')\mathbf{r}'}|\psi_{n\mathbf{k}}\rangle \times\left(\frac{1}{\omega+\omega'-\epsilon_{n'\mathbf{k}-\mathbf{q}}+i\eta\,\mathrm{sgn}(\epsilon_{n'\mathbf{k}-\mathbf{q}}-\mu)} + \frac{1}{\omega-\omega'-\epsilon_{n'\mathbf{k}-\mathbf{q}}+i\eta\,\mathrm{sgn}[\epsilon_{n'\mathbf{k}-\mathbf{q}}-\mu]}\right), \tag{10}$$

where μ is the Fermi energy. The Greens function is never

explicitly stored or evaluated. The frequency grid has been constrained to positive values, observing that the screened potential W is an even function of ω', whereas the Green's function is an odd function of ω'. Furthermore the bare Coulomb kernel $\nu_{\mathbf{q}}^{\mathrm{bare}}$ has been subtracted

$$\bar{W}_{\mathbf{q}}(\mathbf{G},\mathbf{G}',\omega') = W_{\mathbf{q}}(\mathbf{G},\mathbf{G}',\omega') - \nu_{\mathbf{q}}^{\mathrm{bare}}(\mathbf{G},\mathbf{G}'), \quad (11)$$

which makes the integral well behaved, since $W(\omega)$ approaches ν^{bare} at large frequencies. In order to obtain the final self-energy, the exact Fock exchange term must be added concomitantly,

$$\Sigma(\omega)_{n\mathbf{k},n\mathbf{k}} = \bar{\Sigma}(\omega)_{n\mathbf{k},n\mathbf{k}} + \langle\psi_{n\mathbf{k}}|\nu_x|\psi_{n\mathbf{k}}\rangle. \quad (12)$$

In the self-energy, the exchange charge densities $\langle\psi_{n\mathbf{k}}|e^{i(\mathbf{q}+\mathbf{G})\mathbf{r}}|\psi_{n'\mathbf{k}-\mathbf{q}}\rangle$ are again approximated according to Eq. (9). The exchange term $\langle\psi_{n\mathbf{k}}|\nu_x|\psi_{n\mathbf{k}}\rangle$ is calculated using the same description for the exchange charge density, but utilizing the diagonal properties of the bare Coulomb kernel.[30] The frequency integration is carried out using the method described in Appendix A, adopting a suitable frequency grid as described in Appendix B.

Before continuing we note that our implementation differs from that of Arnaud *et al.*[20] in one important aspect. Arnaud *et al.* suggested to develop the difference between the one-center AE and pseudocharge into a Fourier series and to add this difference to the plane-wave pseudo-charge-density in order to restore the properties of the one-center AE charge density on the plane-wave grid [second term in Eq. (9)]. In principle, the total exchange charge density constructed in this way is exact, provided that the AE charge distribution can be represented with the applied basis set. We refer here to the basis set used for the dielectric functions and the exchange charge density [maximum $\mathbf{G}$ in Eq. (9)] and not the usual plane-wave basis set used for the expansion of the wave functions. In practice, however, this requirement cannot be met, since the AE charge distribution contains very high Fourier components. We believe that this can lead to inaccuracies in the evaluation of the exchange and self-energy: for a *finite basis set*, Arnauds approach does not guarantee the proper conservation of the norm or multipole moments inside the atomic spheres. Since the electrostatic interactions are long ranged and prone to errors in the charge distribution, Arnauds approach might lead to inaccuracy in the calculation of the QP energies. Our construction of the exchange charge density—which is in its essence equivalent to the original method of Blöchl for the treatment of the Hartree energy[19]—conserves multipole moments inside the spheres even for small basis sets. We note that the basis sets used by Arnaud for the representation of the dielectric matrix and exchange charge-density distribution are not particularly large (typically 100–200 plane waves).[20]

E. One center terms

Up to this point, we have entirely neglected the PAW one-center terms. Modelling the dielectric function in the spheres is a delicate and complicated issue and would be required in order to obtain a full *GW* PAW implementation. This could be done using the product basis sets suggested in Refs. 12 and 16, but it would make the implementation not only much more involved, but it would also slow the calculations significantly. The approach we adopt here is much simpler and inspired by Massidda, Posternak, and Baldereschi:[43] we assume that the dielectric matrix is diagonal and its diagonal is equal to one whenever terms inside atomic spheres are evaluated.

For the one-center terms, the *GW* Hamiltonian is thus simply approximated by the Hartree-Fock Hamiltonian. This amounts to an evaluation of the Hartree-Fock Hamiltonian for each atomic sphere using first the reconstructed pseudo-wave-functions and then the reconstructed AE wave functions [see Figs. 1(b) and 1(c)]. This approximation is *the crucial one of our present implementation*, but it is expected to be reliable since differences between the pseudo-wave-function and AE wave function are only present for large reciprocal lattice vectors $\mathbf{G}$, and $\epsilon(\mathbf{G},\mathbf{G}',\omega)$ approaches $\delta(\mathbf{G}-\mathbf{G}')$ very rapidly. As in the pseudopotential case, one can make the pseudo-wave-functions more precise by decreasing the core radius used during the generation of the PAW datasets. In the limit of very small radii, the pseudo-wave-function will approach the exact AE wave function, as it does in pseudopotential codes. As shown below, a decrease of the core radius from 1.9 a.u. to 1.6 a.u. for Si $2p$ electrons, or from 2.3 to 1.6 a.u. for Cd $4s$ electrons had practically no influence on the QP shifts. In general, we found that the results are very robust with respect to the core radius, and QP shifts are typically constant within 0.01–0.02 eV, if the core radii are reduced. But we cannot entirely exclude to see a stronger change, for instance, in the more problematic transition metal oxides or in lanthanide oxides. For semiconductors and main group oxides, however, the present approximation seems to give very reliable results to within the quoted 0.02 eV.

It is emphasized that the additive augmentation concept used in the PAW method (i.e. subtracting the pseudo-one-center terms and adding the AE one-center terms) is a prerequisite for the success of this approximation. The approximation would be less reliable in other full-potential methods, such as the FLAPW or FP-LMTO method.

For the one-center terms, the exact all-electron exchange contribution onto a state $\psi_{n\mathbf{k}}$ has been amply discussed in Ref. 30 [see Eq. (31) ff.] and involves the calculation of the following term:

$$\langle\psi_{n\mathbf{k}}|\nu_x^{(1)}|\psi_{n\mathbf{k}}\rangle = -\sum_{n'}\sum_{ij;kl}\langle\tilde{\psi}_{n\mathbf{k}}|\tilde{p}_i\rangle\langle\tilde{p}_k|\tilde{\psi}_{n\mathbf{k}}\rangle\langle\tilde{\psi}_{n'\mathbf{k}}|\tilde{p}_l\rangle\langle\tilde{p}_j|\tilde{\psi}_{n'\mathbf{k}}\rangle \times e^2\int\frac{\phi_i(\mathbf{r})\phi_j(\mathbf{r})\phi_l(\mathbf{r}')\phi_k(\mathbf{r}')}{|\mathbf{r}-\mathbf{r}'|}d^3\mathbf{r}d^3\mathbf{r}', \quad (13)$$

where the sum over n' is performed over all occupied one electron states, and $\phi_i(\mathbf{r})$ is the ith all-electron partial wave. The indices i, j, k, and l contain an atomic site index, and are constrained to a single atom; the integral is evaluated for each atomic sphere separately. The one-center pseudocontributions $\langle\psi_{n\mathbf{k}}|\tilde{\nu}_x^{(1)}|\psi_{n\mathbf{k}}\rangle$ are analogous (see Ref. 30 for details).

F. Treatment of core-valence interaction

In the calculation of the quasiparticle energies [Eq. (4)], one should also include the exchange-correlation contribution from the core-valence interaction—for the sake of consistency—in the *GW* approximation. This contribution can be estimated in the LDA or on the Hartree-Fock level, where the latter one is expected to be more reliable since the *GW* self-energy approaches the bare Fock exchange operator in the short wavelength regime. Within LDA, the core-valence exchange-correlation contribution is calculated as

$$\langle \psi_{n\mathbf{k}} | \nu_{xc\ \text{core-val}}^{\text{LDA}} | \psi_{n\mathbf{k}} \rangle = \langle \psi_{n\mathbf{k}} | \nu_{xc}^{\text{LDA}}(n_v + n_c) - \nu_{xc}^{\text{LDA}}(n_v) | \psi_{n\mathbf{k}} \rangle, \tag{14}$$

where n_v and n_c are the valence and core densities, respectively. This term is calculated in the PAW framework, which involves the calculation of a plane wave and two one-center terms (see Fig. 1) and the final contribution is simply added to the QP energies defined in Eq. (3).

When the core-valence interactions are treated on the Hartree-Fock level, the matrix element is calculated for the all-electron contribution in the atomic spheres analogously to Eq. (13),[20,30]

$$\langle \psi_{n\mathbf{k}} | \nu_{x\ \text{core-val}}^{(1)} | \psi_{n\mathbf{k}} \rangle = -\sum_{ij;c} \langle \tilde{\psi}_{n\mathbf{k}} | p_i \rangle \langle p_j | \tilde{\psi}_{n\mathbf{k}} \rangle \times e^2 \int \frac{\phi_i(\mathbf{r}) \phi_c(\mathbf{r}) \phi_c(\mathbf{r}') \phi_j(\mathbf{r}')}{|\mathbf{r} - \mathbf{r}'|} d^3\mathbf{r} d^3\mathbf{r}', \tag{15}$$

where $\phi_c(\mathbf{r})$ are core-electron orbitals c, centered on the same atom as the partial waves and projectors with the indices i and j. Since our present PAW implementation uses the frozen core approximation, the core wave functions need to be determined consistently with the partial waves of the valence wave functions (orthogonality). This implies that we must use the atomic core wave functions of a previous LDA calculation for the evaluations of Eq. (15).

As a short note, it should be mentioned that the evaluation of the core-valence interactions on the HF level is not possible in the pseudopotential approximation, since, in this case, the charge distribution and the wave functions of the valence electrons in the core region are not physically meaningful.

III. SPECTRAL REPRESENTATION

A. Polarizability using Hilbert transform

The calculation of the polarizability matrix [Eq. (8)] is rather time consuming, as the summation is carried out over all possible pairs of occupied and unoccupied states. Moreover, these summations must be performed for each frequency of the chosen frequency grid. To optimize the computational procedure one can instead calculate the spectral representation of the polarizability,[11]

$$\chi_{\mathbf{q}}^{S}(\mathbf{G},\mathbf{G}',\omega') = \frac{1}{\Omega} \sum_{nn'\mathbf{k}} 2w_{\mathbf{k}}\, \text{sgn}(\omega')\, \delta(\omega' + \epsilon_{n\mathbf{k}} - \epsilon_{n'\mathbf{k}-\mathbf{q}}) \times (f_{n\mathbf{k}} - f_{n'\mathbf{k}-\mathbf{q}}) \langle \psi_{n'\mathbf{k}-\mathbf{q}} | e^{-i(\mathbf{q}+\mathbf{G})\mathbf{r}} | \psi_{n\mathbf{k}} \rangle \times \langle \psi_{n\mathbf{k}} | e^{i(\mathbf{q}+\mathbf{G}')\mathbf{r}'} | \psi_{n'\mathbf{k}-\mathbf{q}} \rangle, \tag{16}$$

where the spectral function is related to the imaginary part of the polarizability through

$$\chi_{\mathbf{q}}^{S}(\mathbf{G},\mathbf{G}',\omega') = \frac{1}{\pi}\, \text{Im}\, \chi_{\mathbf{q}}^{0}(\mathbf{G},\mathbf{G}',\omega).$$

Evaluation of the spectral function at a frequency ω' is rather efficient, as the only states that must be included in the summation are those that satisfy the criteria $\omega' + \epsilon_{n\mathbf{k}} - \epsilon_{n'\mathbf{k}-\mathbf{q}} = 0$ for a given frequency ω'. Or from another point of view, each pair of states $n\mathbf{k}, n'\mathbf{k}-\mathbf{q}$ contributes to χ only at the frequency $\omega' = \epsilon_{n'\mathbf{k}-\mathbf{q}} - \epsilon_{n\mathbf{k}}$.

The polarizability is calculated on a discrete grid of frequencies, and the δ-function in (16) is approximated by a triangular function centered at $\Delta_{n'n} = \epsilon_{n'\mathbf{k}-\mathbf{q}} - \epsilon_{n\mathbf{k}}$ in the following manner: at a given frequency ω_i, the triangular function is nonzero only if $\omega_{i-1} < \Delta_{n'n} < \omega_{i+1}$. If the energy difference $\Delta_{n'n}$ lies in one such interval, the δ function is approximated as

$$\delta(\omega_i - \Delta_{n'n}) \rightarrow \begin{cases} \dfrac{\Delta_{n'n} - \omega_{i-1}}{\omega_i - \omega_{i-1}} & \text{for } \omega_{i-1} < \Delta_{n'n} \leqslant \omega_i, \\ \dfrac{\omega_{i+1} - \Delta_{n'n}}{\omega_{i+1} - \omega_i} & \text{for } \omega_i \leqslant \Delta_{n'n} < \omega_{i+1}. \end{cases} \tag{17}$$

The triangular function is equal to one for $\epsilon_{n'\mathbf{k}-\mathbf{q}} - \epsilon_{n\mathbf{k}} = \omega_i$ and approaches zero, if $\epsilon_{n'\mathbf{k}-\mathbf{q}} - \epsilon_{n\mathbf{k}}$ is close to either ω_{i-1} or ω_{i+1}. With this definition, the frequency grid is not restricted to a linear form, and the norm of the delta function is automatically exactly conserved. The representation is inspired by finite element basis sets and can be readily extended to higher order Lagrange polynomials. But we note that the nonanalytic behavior of the polarizability makes higher order interpolation procedures not necessarily more accurate.

The polarizability matrices are obtained from the spectral function by the following Hilbert or Kramers-Kronig transform:

$$\chi_{\mathbf{q}}^{0}(\mathbf{G},\mathbf{G}',\omega) = \int_0^\infty d\omega'\, \chi_{\mathbf{q}}^{S}(\mathbf{G},\mathbf{G}',\omega') \times \left(\frac{1}{\omega - \omega' - i\eta} - \frac{1}{\omega + \omega' + i\eta} \right), \tag{18}$$

with frequencies ω and ω' that, in the general case, could be defined on different frequency grids, but are chosen to belong to the same set in the present implementation. The Hilbert transform is performed using a triangular finite element basis set, as described in Appendix A.

In the described method, one must carry out a single loop over all pair of states $n\mathbf{k}, n'\mathbf{k}-\mathbf{q}$, determine the largest frequency ω_i' that observes $\omega_i' < \epsilon_{n'\mathbf{k}-\mathbf{q}} - \epsilon_{n\mathbf{k}}$, and add contribu-

tions to the spectral function $\chi^S_{\mathbf{q}}(\mathbf{G},\mathbf{G}',\omega')$ [Eq. (16)] at ω'_i and ω'_{i+1} using proper weights [Eq. (17)]. For this procedure, the computational effort does not depend on the density of the frequency grid, and it is exactly twice as large as for static calculations. The Kramers-Kronig transformation however scales quadratically with the number of frequencies. In practice, we found its computational time to be one order of magnitude smaller than for the evaluation of Eq. (16).

The presented procedure for the calculation of the frequency-dependent polarizability matrices is similar to the method of Miyake and Aryasetiawan,[11] with the difference that they represented the δ functions using Gaussian contours centered at the energy point $\epsilon_{n'\mathbf{k}-\mathbf{q}}-\epsilon_{n\mathbf{k}}$. Our methodology, identical in its essence to that of Miyake and Aryasetiawan,[11] seems to be more straightforward in its implementation, since it avoids Taylor expansions of the exponential function and summation over the moments of the expansion.

B. Self-energy using Hilbert transforms

The evaluation of the self-energy [Eq. (10)] is equally time consuming. At a first glance, two possible methods can be adopted. Either, one first starts by contracting all $\mathbf{G}$ and $\mathbf{G}'$-dependent quantities in a summation over $\mathbf{G}$ and $\mathbf{G}'$,

$$\Lambda_{n\mathbf{k},n'\mathbf{k}-\mathbf{q}}(\omega') = \frac{1}{\Omega}\sum_{\mathbf{G}\mathbf{G}'} W_{\mathbf{q}}(\mathbf{G},\mathbf{G}',\omega')\langle\psi_{n\mathbf{k}}|e^{i(\mathbf{q}+\mathbf{G})\mathbf{r}}|\psi_{n'\mathbf{k}-\mathbf{q}}\rangle \times\langle\psi_{n'\mathbf{k}-\mathbf{q}}|e^{-i(\mathbf{q}+\mathbf{G}')\mathbf{r}'}|\psi_{n\mathbf{k}}\rangle. \tag{19}$$

Then, the self-energy can be evaluated with relatively modest computational effort as a Hilbert transform of $\Lambda_{n\mathbf{k},n'\mathbf{k}-\mathbf{q}}(\omega')$:

$$\Sigma(\omega)_{n\mathbf{k},n\mathbf{k}} = \sum_{n'}\frac{i}{2\pi}\int_{-\infty}^{\infty} d\omega' \times \frac{\Lambda_{n\mathbf{k},n'\mathbf{k}-\mathbf{q}}(\omega')}{\omega+\omega'-\epsilon_{n'\mathbf{k}-\mathbf{q}}+i\eta\,\mathrm{sgn}(\epsilon_{n'\mathbf{k}-\mathbf{q}}-\mu)}. \tag{20}$$

We have adopted this method, if the full frequency-dependent self-energy is required. The calculation of the function Λ is by far the most time-consuming part for the determination of the quasiparticle energies, and savings must concern this part in order to be effective.

The second procedure inverts the order of execution and starts from the Hilbert transform of the frequency-dependent screened interaction

$$C_{\mathbf{q},n'\mathbf{k}-\mathbf{q}}(\mathbf{G},\mathbf{G}',\omega) = \frac{i}{2\pi}\int_{-\infty}^{\infty} d\omega' \times \frac{W_{\mathbf{q}}(\mathbf{G},\mathbf{G}',\omega')}{\omega+\omega'-\epsilon_{n'\mathbf{k}-\mathbf{q}}+i\eta\,\mathrm{sgn}(\epsilon_{n'\mathbf{k}-\mathbf{q}}-\mu)}, \tag{21}$$

with a final evaluation of the self-energy using a similar equation as in (19). The second route is more time consuming than the first, as it requires a Hilbert transform of the screened potential matrix $W(\omega')$ [Eq. (21)] for each state $n'\mathbf{k}-\mathbf{q}$, in contrast to the Hilbert transform of the functions $\Lambda_{n\mathbf{k},n'\mathbf{k}-\mathbf{q}}(\omega')$ [Eq. (20)], which usually possess less elements than $W_{\mathbf{q}}(\mathbf{G},\mathbf{G}',\omega')$. The problematic point is the dependency on the eigenenergy $\epsilon_{n'\mathbf{k}-\mathbf{q}}$ in the denominator of the preceding equation.

An alternative and admittedly less obvious approach, which does not require to carry out Hilbert transforms for each state n', can be obtained by substituting $\bar{\omega}=\omega-\epsilon_{n'\mathbf{k}-\mathbf{q}}$. In this case the Hilbert transform needs to be carried out only once for positive and negative complex shifts as

$$C^{\pm}_{\mathbf{q}}(\mathbf{G},\mathbf{G}',\bar{\omega}) = \frac{i}{2\pi}\int_0^{\infty} d\omega' W_{\mathbf{q}}(\mathbf{G},\mathbf{G}',\omega') \times\left(\frac{1}{\bar{\omega}+\omega'\pm i\eta}+\frac{1}{\bar{\omega}-\omega'\pm i\eta}\right). \tag{22}$$

In the current implementation of Eq. (22), $\bar{\omega}$ lies on the same frequency grid as other quantities. For each matrix $C^{+}_{\mathbf{q}}(\mathbf{G},\mathbf{G}',\bar{\omega})$ and $C^{-}_{\mathbf{q}}(\mathbf{G},\mathbf{G}',\bar{\omega})$, the screened two-electron integrals are defined as

$$S^{\pm}_{n\mathbf{k},n'\mathbf{k}-\mathbf{q}}(\bar{\omega}) = \frac{1}{\Omega}\sum_{\mathbf{G},\mathbf{G}'} C^{\pm}_{\mathbf{q}}(\mathbf{G},\mathbf{G}',\bar{\omega})\langle\psi_{n\mathbf{k}}|e^{i(\mathbf{q}+\mathbf{G})\mathbf{r}}|\psi_{n'\mathbf{k}-\mathbf{q}}\rangle \times\langle\psi_{n'\mathbf{k}-\mathbf{q}}|e^{-i(\mathbf{q}+\mathbf{G}')\mathbf{r}'}|\psi_{n\mathbf{k}}\rangle. \tag{23}$$

The self-energy at $\epsilon_{n\mathbf{k}}$ can be finally calculated as a sum of these screened two-electron integrals

$$\langle\psi_{n\mathbf{k}}|\Sigma(\epsilon_{n\mathbf{k}})|\psi_{n\mathbf{k}}\rangle = \sum_{n'\mathbf{k}-\mathbf{q}} \mathrm{sgn}(\epsilon_{n\mathbf{k}}-\epsilon_{n'\mathbf{k}-\mathbf{q}}) \times S^{\mathrm{sgn}(\epsilon_{n'\mathbf{k}-\mathbf{q}}-\mu)\mathrm{sgn}(\epsilon_{n\mathbf{k}}-\epsilon_{n'\mathbf{k}-\mathbf{q}})}_{n\mathbf{k},n'\mathbf{k}-\mathbf{q}}(|\epsilon_{n\mathbf{k}}-\epsilon_{n'\mathbf{k}-\mathbf{q}}|). \tag{24}$$

Because the screened two electron integrals are originally calculated at a discrete set of frequencies $\bar{\omega}_i$, the values of S^+ or S^- at the points $\Delta_{nn'}=\epsilon_{n\mathbf{k}}-\epsilon_{n'\mathbf{k}-\mathbf{q}}$ need to be obtained by a linear interpolation from those two frequency points of the grid which are closest to the energy $\Delta_{nn'}$,

$$S^{\pm}(|\Delta_{nn'}|) = \theta(|\Delta_{nn'}|-\bar{\omega}_i)\theta(\bar{\omega}_{i+1}-|\Delta_{nn'}|) \times\left(\frac{\bar{\omega}_{i+1}-|\Delta_{nn'}|}{\bar{\omega}_{i+1}-\bar{\omega}_i}S^{\pm}(\bar{\omega}_i)+\frac{|\Delta_{nn'}|-\bar{\omega}_i}{\bar{\omega}_{i+1}-\bar{\omega}_i}S^{\pm}(\bar{\omega}_{i+1})\right). \tag{25}$$

The above expression is given for absolute values of $\Delta_{nn'}$. For negative $\Delta_{nn'}$, the following simple transformations are used for S^+ or S^- to write them as functions of positive frequencies:

$$S^{\pm}_{n\mathbf{k},n'\mathbf{k}-\mathbf{q}}(-|\Delta_{nn'}|) = -S^{\mp}_{n\mathbf{k},n'\mathbf{k}-\mathbf{q}}(|\Delta_{nn'}|). \tag{26}$$

The sign of $\Delta_{nn'}$ is already accounted for in Eq. (24).

The last approach is particularly fast for the evaluation of QP shifts using Eq. (5). For the evaluation of $\Sigma(\epsilon_{n\mathbf{k}})$ and $\partial\,\mathrm{Re}\,\Sigma(\epsilon_{n\mathbf{k}})/\partial\epsilon_{n\mathbf{k}}$, one needs to evaluate the screened two

TABLE I. Core radii r_c and typical energy cutoffs E for the PAW potentials used in the present work. If the core radii for different quantum numbers are different, they are specified using a subscript. Nonlocal projectors were generated for the states indicated in the column "val." As local potential a pseudopotential was generated for the states indicated in the column "local." The number of frequencies N_ω used in the *GW* calculations for each material is provided as well. The norm conserving Troullier-Martins potential for Si is marked as Si-TM (Ref. 41).

	val	local	r_c(a.u.)	E(eV)	N_ω
Si-TM	$3s3p$	$3d$	2.1	350	300
Si	$3s3p3d$	$4f$	1.9	250	300
Si-2p	$2p3s3p3d$	$4f$	$1.6_p, 1.9_{sd}$	430	500
Ga	$4s4p$	$4f$	2.6	140	300
Ga-3d	$3d4s4p$	$4f$	2.3	310	300
Ga-3pd	$3p3d4s4p$	$4f$	$1.7_p, 2.0_{sd}$	380	500
Ga-3spd	$3s3p3d4s4p$	$4f$	$1.4_s, 1.7_{pd}$	500	500
As	$4s4p$	$4f$	2.1	210	
Cd-4d	$4d5s$	$4f$	$2.3_{sp}, 2.0_d$	370	300
Cd-4pd	$4p4d5s$	$4f$	$2.3_s, 1.7_p, 1.9_d$	400	500
Cd-4spd	$4s4p4d5s$	$4f$	1.6	660	500
S	$3s3p$	$4f$	1.9	260	

electron integrals (23) not at all frequencies of the grid $\bar{\omega}_i$, but only at those two frequencies which are closest to $\epsilon_{n\mathbf{k}} - \epsilon_{n'\mathbf{k}-\mathbf{q}}$. In practice, this is simple to implement. As for the polarizability, a loop over all pairs of states $n\mathbf{k}, n'\mathbf{k}-\mathbf{q}$ is performed, the energy difference $\Delta_{nn'}$ is calculated, the largest frequency ω_i that observes $\omega_i < \Delta_{nn'}$ is determined, and the screened two electron integral is evaluated for this frequency ω_i and ω_{i+1}. Thus, the number of operations is *independent of the frequency grid and twice as large as for a purely static calculation*.

IV. RESULTS FOR QUASIPARTICLE ENERGIES

A. Technical details

The details of the PAW potentials used in the present work are presented in Table I. These potentials differ from the "standard" PAW potentials—as supplied in the VASP package and normally used in DFT calculations—by an accurate description of scattering properties even at very high energies. The scattering properties were evaluated for spherical atoms. As an example, Fig. 2 provides the logarithmic derivatives for the s, p, and d wave functions at a radius equal to one-half the interatomic distance as a function of the energy, for a norm-conserving Troullier-Martins Si potentials (Si-TM) (Ref. 41) and the Si PAW potential. Such a plot is usually used to evaluate the performance of pseudopotentials, and the magnitude of the deviation between the pseudopotential (PAW) results (dotted lines) and all-electron calculations (filled lines) allows to determine how well the scattering properties are reproduced at the considered energy. Up to 1 Ry above the vacuum level, the scattering properties for both potentials are in close agreement with each other and with the exact AE results. This is sufficient for ground state DFT calculations, and even the static dielectric properties are hardly affected by the discrepancies of the Si TM potential at higher energies. However, the TM potential shows marked deviations from the AE results above 1 Ry, in particular, for s, and to a lesser extend, for p like waves. An important consequence of this deviation is that states 1 Ry above the Fermi level tend to be bound too strongly by the TM potential. For the PAW potential no deviations are visible, but we note that we had to take into account d projectors in order to obtain this agreement with the AE values. Additionally, we have used two partial waves for the s, p, and d states; one in the valence band and a second one roughly 6 Ry above the vacuum level. This allows to "pinpoint" the scattering properties at these two energies exactly. In principle, it would be even possible to add a third nonlocal projector in order to improve the scattering properties at even higher energies, but this has not been attempted in the present work.

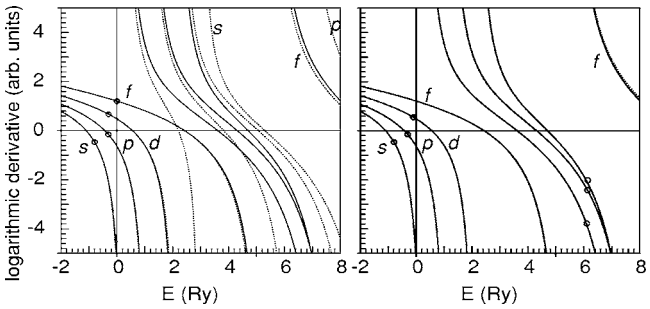

FIG. 2. Atomic scattering properties of the Si TM (left) and PAW (right) potentials used in the present work for QP calculations (Tables I and II). Shown are the logarithmic derivatives of the radial wave functions for different angular momenta for a spherical Si atom, evaluated at a distance of r=1.3 Å from the nucleus. Solid lines correspond to the all-electron full-potential, and dotted lines to the TM pseudopotential or PAW potential. The energy zero corresponds to the vacuum level. Circles indicate linearization energies for projectors.

TABLE II. Quasiparticle energies for Si referenced to Γ_{25v} using LDA and G_0W_0 and various potentials. The core-valence (c-val) interaction is treated either on the LDA (left) or HF level (right). The FP-LMTO results of Kotani *et al.* (Refs. 16 and 44) and the AE-PP calculations of Tiago *et al.* (Ref. 6) and experimental values are also shown. Details for potentials are given in Table I.

Method Potential c-val	LDA Si LDA	LDA Si-TM LDA	*GW* Si-TM LDA	*GW* Si LDA	*GW* Si HF	*GW* Si-2*p* HF	*GW* (Refs. 16 and 44) FP-LMTO HF	*GW* (Ref. 42) FLAPW	*GW* (Ref. 6) AE-PP	Expt. (Ref. 34)
Γ_{1v}	−11.97	−11.97	−11.62	−11.75	−11.85	−11.87				−12.5±0.6
Γ_{25v}	0.00	0.00	0.00	0.00	0.00	0.00		0.00		0.0
Γ_{15c}	2.52	2.53	3.23	3.17	3.17	3.16	3.12	3.20	3.24	3.40
Γ_{2c}	3.20	3.10	3.82	4.04	4.01	3.97				4.23
X_{1v}	−7.82	−7.81	−7.60	−7.68	−7.76	−7.77				
X_{4v}	−2.86	−2.85	−2.83	−2.88	−2.91	−2.90		−2.92		
X_{1c}	0.60	0.62	1.33	1.19	1.15	1.14	0.98	1.19	1.18	1.25
X_{3c}	9.98	9.94	10.44	10.54	10.64	10.61				
L_{2v}	−9.63	−9.62	−9.37	−9.46	−9.55	−9.59				−9.3±0.4
L_{1v}	−7.00	−6.99	−6.78	−6.87	−6.94	−6.94				−6.7±0.2
L_{3v}	−1.20	−1.20	−1.20	−1.22	−1.23	−1.23		−1.23		−1.2±0.2
L_{1c}	1.43	1.41	2.10	2.10	2.07	2.04		2.12		2.4±0.15
L_{3c}	3.29	3.31	4.05	3.93	3.93	3.92				

Table I provides the core radii of the potentials, the energy cutoffs for the plane-wave basis sets, the number of the frequencies used in the *GW* calculations and highlights the states treated as valence. For compounds, calculations were performed at the higher energy cutoff of the two elements involved. Two projectors are used for any of the l quantum numbers listed in the column "val." For all *GW* calculations, 160 electronic bands were used, as this number gives reasonably well converged results and is also close to the values used in other presentations.[6,10] A $6\times6\times6$ k-point grid centered at the Γ-point was used for all tabulated values. The number of frequency points used for the calculations of GaAs and CdS are given only for the potentials of Ga and Cd. Note that potentials with deep lying semicore states treated as valence (e.g., Ga-*sv*) require more frequency grid points in order to achieve convergence. Tests indicate that the applied frequency grids yield converged results with respect to all specified digits (better than 0.01 eV). Throughout all *GW* calculations we used a complex shift of 0.1 eV for the calculation of the dielectric matrices and self-energies. We report only single shot G_0W_0 values and they have been calculated using Eq. (4). Furthermore the experimental (room temperature) lattice constants were applied throughout all calculations: 5.43 Å for Si, 5.65 Å for GaAs, and 5.85 Å for CdS.

The basis set size for the response functions and W was chosen to include all plane waves up to an energy cutoff of 250 eV. At 250 eV the diagonal components of the dielectric function is already converged to one, and the results are insensitive to an increase of the cutoff. The exchange integrals were calculated using much larger basis sets, with plane-wave cutoffs exceeding those used for the wave functions.

B. GW quasiparticle energies of Si

To test our implementation, we carried out *GW* calculations for Si, since the results for this material can be compared to an abundant amount of data provided by previous *GW* calculations and experimental results. Calculations reveal that the eigenvalues of the LDA calculations change only by 0.02 eV from $(4\times4\times4)$ to $(6\times6\times6)$ k points. The *GW* eigenvalues show satisfactory k-point convergence as well (the change of the gap is only 0.03 eV), with the exception of the bottom of the valence band (Γ_{1v} and L_{2v}), which differs by more than 0.2 eV between the two k-point sets. Using $(8\times8\times8)$ k points the conduction bands change by at most 5 meV and the bottom of the valence band by 20 meV. Hence our reported values are essentially k-point converged. We note that the head and wings of the dielectric matrix are calculated exactly, which is important for fast convergence. Calculations also show that the treatment of core-valence interactions using DFT or HF does not alter the eigenvalues significantly, indicating that the core-valence interaction is small for Si (see below).

The results for various PAW potentials and the norm conserving Troullier-Martins pseudopotential[41] are shown in Table II. The LDA eigenenergies are identical for all three potentials to within typically 0.02 eV, except for the Γ_{2c} and X_{3c} point, for which the TM potential underestimates the energies by 0.1 and 0.05 eV, respectively. The indirect *GW* gap $\Gamma_{25v}-X_{1c}$ calculated using the norm-conserving valence-only TM potential is close to values reported before for other G_0W_0 pseudopotential calculations (1.31 eV for 186 bands),[10] but the gap and other eigenvalues differ by up to 0.2 eV from the PAW calculations. Two reasons are responsible for the observed discrepancies. First, in the TM pseudopotential calculation, we need to treat the core-valence interaction on the LDA level. As Table II indicates, this accounts for roughly half of the discrepancy (difference between, *GW*-Si-LDA and *GW*-Si-HF). We note that our TM potential incorporates nonlinear core corrections as suggested by Louie.[40] Omitting these corrections increases the gap even

further to 1.41 eV, and places the bottom of the valence band at −11.57 eV.

The remaining discrepancies were difficult to disentangle, but generating PAW potentials with only a single projector per angular quantum number and norm-conserving potentials with two projectors, we concluded, that one-half of the remaining discrepancy is related to the inaccurate description of the scattering properties at high energies (typically 0.05 meV), and the remainder is related to the inaccurate representation of the valence wave functions close to the core. These effects are, however, to some extent interconnected.

We conclude that valence only pseudopotentials typically incur errors of the order of 0.1–0.2 eV even for a material with a fairly small core-valence interaction. For norm-conserving pseudopotential, it is possible to improve the scattering properties and the description of the charge distribution by carefully adjusting the core radii and unfreezing shallow core states (e.g., 2*s* and 2*p*). By doing this Tiago *et al.* obtained a QP energy of 1.18 eV at X_{1c} using a norm-conserving pseudopotential, in good agreement with the present results.[6] It is likely that such a small core potential yields an excellent description of high lying conduction band states and of the charge distribution close to the core. It remains to be demonstrated that the core states (2*s* and 2*p*) influence the results only little in the PAW case, in particular, in view of a recent work claiming that the results are sensitive to whether the 2*s* and 2*p* electrons are treated as core or valence states.[35] In order to test this, we have moved the 2*p* shell into the valence and simultaneously decreased the core radius to 1.6 a.u. As Table II shows, this has a negligible influence on the gap (decreases by 0.015 eV), and a slight downshift of the lower valence band edge (Γ_{1v}) by 0.02 eV is observed. By any practical means such a change is small considering the errors incurred by the G_0W_0 approximation itself.

We believe that the present values are essentially converged with respect to the number of *k* points and with respect to other technical parameters (frequency grid, complex shift). There is some room for further improvement, by increasing the number of conduction bands in the *GW* calculation, and we indeed obtain a value of 1.173 (2*p* in core) and 1.162 eV (2*p* in valence) at X_{1c} using 250 bands and $6\times6\times6$ *k* points. This value is still somewhat smaller than experiment.[34] Our present values are in between previous "all-electron" pseudopotential values by Tiago *et al.* and other all-electron calculations [X_{1c}: FLAPW 1.14 eV,[23] FLAPW 1.00 eV,[35] FP-LMTO 0.98 eV,[44] PAW 1.01 eV (Ref. 21)]. The reason for the large deviations between the all-electron calculations are yet unknown, but Friedrich *et al.* has recently pointed out that the linearized basis sets used in the FLAPW and FP-LMTO method are not sufficiently large to allow an accurate treatment of high lying conduction band states.[42] They obtained a value of 1.19 eV (2*p* in core) and 1.17 (2*p* in valence) using $6\times6\times6$ *k* points, 250 bands and augmenting the usual FLAPW basis set with higher energy derivatives of the one-center wave functions (local orbitals). In their case *k*-point converges was slightly slower, because they calculate the head of the matrix using finite differences, and their *k*-point converged values are reported to be 0.02 eV smaller than those using $6\times6\times6$ *k* points (1.17 2*p* in core, and 1.15 2*p* in valence). The *k*-point converged values are hence identical to our values.

C. GW quasiparticle energies of GaAs and CdS

The second important test case is GaAs. Here we want to demonstrate that a treatment of the core valence interaction on the Hartree-Fock level is highly desirable and allows to keep most electrons in the core.

The LDA and quasiparticle eigenvalues of GaAs are presented in Table III. In distinction to Si, even the LDA eigenvalues of GaAs are sensitive to how many electrons are treated as valence electrons. The LDA gap, calculated treating only the three outermost electrons of Ga as valence (0.39 eV) is very close to most previous pseudopotential calculations (e.g., 0.40 eV).[33] If the 3*d* electrons are treated as valence electrons, the gap shrinks by 0.1 eV and we obtain an LDA gap of 0.31 eV. Moving the 3*p* electrons into the valence as well has little influence on the gap (0.32 eV). We have found the same gap using the APW+*lo* method, as implemented in the WIEN2K program,[39] in agreement with some other previous FP-LMTO calculations.[16]

We now concentrate on the *GW* gaps, when the core-valence interaction is evaluated on the HF level (right-hand side of Table III). As for DFT/LDA calculations, the fundamental gap Γ_{15c} is slightly larger, if the Ga 3*d* shell is treated as a core shell; unfreezing the shell yields a reduction by 0.12 eV. If the 3*p* shell is treated as valence as well, no further change is observed for the valence electrons, whereas the 3*d* level shifts upwards. We explain this by a screening of the exchange interaction between the 3*p* and 3*d* electrons: if the 3*p* electrons are placed in the core, the bare exchange interaction between the 3*p* and 3*d* shell is implicitly used (Hartree-Fock), whereas, when the 3*p* electrons are treated as valence electrons, the interaction can be screened by the other valence electrons, causing an upshift of the 3*d* orbitals. This upshift, however, has no effect on the valence electrons, and we also note that treating the 3*s* shell as valence caused no further change of the position of the 3*d* states or the band gap.

In the case of GaAs we observe excellent agreement with AE full-potential calculations. The fundamental gap is slightly smaller in our case, and the gap at the *X* point is somewhat larger. Similar tests as presented here—successive un-freezing of lower core shells—have also been performed by Kotani *et al.*[16] They found similar trends, but their results were slightly more sensitive to the number of electrons treated as core electrons. We initially found a similar "scatter," and only when we carefully inspected the logarithmic energy derivatives at high energies (6 Ry above the vacuum level of the atom) and constructed all potentials to have essentially identical high energy scattering properties, consistent results were obtained. We therefore believe that their small deviations are related to differences in the representation of high lying conduction band states, which are difficult to treat in any linear method.[42]

We now turn to the results obtained, when treating the core-valence interaction on the LDA level (left-hand part of

TABLE III. Quasiparticle energies for GaAs referenced to Γ_{25v} using LDA and G_0W_0 and various potentials. The core-valence (c-val) interaction is treated either on the HF or LDA level. The FP-LMTO calculations of Kotani *et al.* (Ref. 16) and the AE-PP calculations of Tiago *et al.* (Ref. 6) and experimental values are also shown.

val. Ga pot c-val	LDA Ga-3*d* LDA	*GW* Ga LDA	*GW* Ga-3*d* LDA	*GW* Ga-3*pd* LDA	*GW* Ga HF	*GW* Ga-3*d* HF	*GW* Ga-3*pd* HF	*GW* (Ref. 16) FP-LMTO HF	*GW* (Ref. 6) AE-PP	Expt. (Refs. 36 and 37)
Γ_{12d}	−14.94		−13.61	−16.57		−18.85	−18.34	−18.1		−18.8
Γ_{1v}	−12.79	−12.71	−12.76	−12.64	−12.58	−12.64	−12.63			
Γ_{25v}	0.00	0.00	0.00	0.00	0.00	0.00	0.00			
Γ_{15c}	0.31	0.93	1.42	1.46	1.38	1.26	1.28	1.30	1.38	1.52
Γ_{2c}	3.65	4.19	4.40	4.35	4.29	4.19	4.20	4.31		
X_{1v}	−10.28	−10.31	−10.26	−10.28	−10.20	−10.26	−10.23			
X_{4v}	−2.72	−2.81	−2.83	−2.77	−2.73	−2.77	−2.76			
X_{1c}	1.33	1.76	1.78	1.79	1.76	1.72	1.71	1.65	1.83	1.98
X_{3c}	1.54	2.01	2.23	2.25	2.06	2.02	2.02	1.99		
L_{2v}	−11.02	−11.07	−10.98	−11.00	−10.95	−11.04	−11.01			
L_{1v}	−6.72	−6.77	−6.58	−6.51	−6.62	−6.67	−6.66			
L_{3v}	−1.16	−1.23	−1.20	−1.18	−1.16	−1.19	−1.18			
L_{1c}	0.84	1.38	1.74	1.76	1.63	1.53	1.55	1.55	1.65	1.82
L_{3c}	4.57	5.11	5.21	5.18	5.08	5.04	5.04			

Table III). When the 3*d* electrons are treated as core, the results are improved with respect to LDA, but the band gaps still tend to be underestimated. Un-freezing the 3*d* shell only, does help but results are still not identical to the previous calculations, and even if the 3*p* shell is treated as valence, results deviate from the AE *GW* calculations. Only if the 3*s* shell is unfrozen as well, the values for the core-valence HF treatment are almost recovered (Γ_{15c} 1.28 eV, X_{1c} 1.79 eV, L_{1c} 1.64 eV). These values are also close to other pseudopotential calculations in which the Ga 3*d*, 3*p*, and 3*s* shells were treated as valence (Ref. 6, Γ_{15c} 1.38 eV, X_{1c} 1.83 eV, L_{1c} 1.65 eV). It is however also clear that such calculations are much too time consuming for routine type calculations even in the PAW case, and a more robust and computationally cheap approach is the evaluation of the core-valence interaction on the HF level. This yields converged results, if the 3*d* shell is treated as valence, but even if the 3*d* shell is kept in the core, satisfactory results are obtained.

For CdS we performed similar tests as for GaAs, but here we only report on the results for the core-valence interaction treated on the HF level (Table IV). The important difference between GaAs and CdS is that the 4*d* shell is located inside the valence band for CdS. We therefore expect that a precise treatment of the 4*d* shell is more important in CdS than in GaAs. Three potentials were constructed unfreezing the 4*d*, 4*p*4*d*, and 4*s*4*p*4*d* electrons, respectively. Simultaneously the core radius was progressively decreased. We first note that the final two potentials Cd-4*pd* and Cd-4*spd* yield identical results. Decreasing the core radius to 1.6 a.u. (Cd -4*spd* case) had no noticeable effect, but it illustrates that our results are robust with respect to the chosen core radii. With the 4*p* states in the valence the Cd 4*d* states are less strongly bound (−8.19 eV compared to −8.35 eV). As for GaAs, the *d* electron levels shift upwards, if the 4*p* electrons are treated as valence. We again explain this by a screening of the core-core exchange interaction by valence electrons. Opposed to GaAs, the precise position of the *d* band also influences the band gap, which is slightly smaller for the final two potentials.

For Cd our results are not in good agreement with previous pseudopotential calculations (we are not aware of AE values).[25] But given the robustness of our results we tend to believe that the results of Fleszar *et al.* were impaired by either their local basis sets or by an inaccurate description of the scattering properties at high energies (details about the pseudopotential construction were not given by the authors).

V. CONCLUSIONS

This paper provides details on the implementation of the *GW* methodology in the PAW framework. The advantages of the PAW method over the pseudopotential approach are threefold: first, it allows to treat *d* and *f* electrons with relatively modest effort. Second, it permits to represent the valence wave functions accurately without any shape approximation, and finally it allows to reevaluate the core-valence interaction on the Hartree-Fock level. In the present implementation, the plane-wave terms (pseudo-wave-functions) are treated exactly, whereas a simple approximation is used for the one-center terms: within the PAW spheres, the *GW* Hamiltonian is approximated by the Hartree-Fock Hamiltonian. This approximation is expected to be reliable since differences between the pseudo-wave-functions and AE wave-functions are only present for large reciprocal lattice vectors $\mathbf{G}$, and $\epsilon(\mathbf{G},\mathbf{G}',\omega)$ approaches $\delta(\mathbf{G}-\mathbf{G}')$ very rapidly. In practice, the incurred errors were not noticeable and are most likely smaller than 0.02 eV.

TABLE IV. Quasiparticle energies for CdS referenced to Γ_{15v} using LDA and G_0W_0 and various potentials. The core-valence interaction is calculated on HF level only. For comparison, the pseudopotential values of Fleszar *et al.* (Ref. 25) are provided.

Valence	LDA	*GW* Cd-4*d*	*GW* Cd-4*dp*	*GW* Cd-4*spd*	*GW* (Ref. 25) Cd-4*spd*	Expt. (Ref. 38)
Γ_{1v}	−12.29	−12.06	−12.10	−12.08	−11.84	
Γ_{15d}	−7.74	−8.35	−8.19	−8.18	−8.29	−9.20
Γ_{12d}	−7.28	−7.99	−7.79	−7.79	−7.88	
Γ_{15v}	0.00	0.00	0.00	0.00	0.00	
Γ_{1c}	0.87	1.92	1.82	1.81	2.13	2.48
X_{1v}	−11.73	−11.64	−11.65	−11.65	−11.37	
X_{3v}	−4.01	−3.91	−3.95	−3.96	−3.94	
X_{5v}	−1.90	−1.92	−1.93	−1.94	−1.92	
X_{1c}	3.32	4.41	4.37	4.37	4.54	
L_{1v}	−11.86	−11.74	−11.75	−11.74	−11.48	
L_{1v}	−4.46	−4.32	−4.37	−4.38	−4.37	
L_{3v}	−0.76	−0.79	−0.79	−0.80	−0.78	
L_{1c}	2.76	4.00	3.91	3.89	4.13	

Similar to the method presented earlier by Miyake and Aryasetiawan[11] we achieve very rapid fully frequency dependent *GW* calculations using a spectral representation of the polarizability and Kramers-Kronig transformations to obtain the real part of the polarizability. This decreases the computational requirement to that for the static case. Moreover, we have extended this method to QP energies, allowing the evaluation of QP shifts with a computational effort that hardly differs from *GW* calculations invoking the plasmon pole approximation.

In Table V we summarize the computational time required to perform single shot G_0W_0 calculations for the materials considered in the present work. The timings include the calculation of the QP shifts at all k points for twice as many electrons as treated as valence. These timings can be further improved, without noticeable changes of the QP energies, by decreasing the cutoffs for the response functions, using smaller fast Fourier transformation grids or by decreasing the number of frequency points (for the grids used in the present work, the Hilbert transforms and inversions of the dielectric matrices require already 30%–50% of the compute time). After optimizing the computational parameters in this manner for Si, we were able to obtain values within 0.01 eV of the reported ones in only 900 seconds (100 frequency points, 150 eV cutoff for response function). Furthermore, using $4\times4\times4$ k points and 100 bands, the calculation takes only a very affordable 100 seconds and errors for the top of the valence and bottom of the conduction band remain below 0.02 eV. Using a similar setup, calculations for a 64 atom Si supercell are possible in less than one day on 4 Opteron nodes, which opens the possibility to perform systematic studies of impurity levels and band offsets in real materials.

TABLE V. Computational time required to calculate QP shifts using 160 bands and $6\times6\times6$ k points (16 k points in IRZ) on a dual processor Opteron 250 (in seconds). Timings are comparable on a single CPU 3.4 GHz P4. For Ga-3*d* and Cd-4*d* only the 4*d* shell has been treated as valence, whereas for Cd-4*pd* the 4*p* shell has been treated as valence as well.

Si	3500 s
Ga-3*d* As	8700 s
Cd-4*d* S	10 600 s
Cd-4*pd* S	19 000 s

We have presented QP shifts for three materials, Si, GaAs, and CdS. In order to obtain converged G_0W_0 results, high lying core shells were successively unfrozen until the results became stable. This gives confidence that we have been able to calculate the true "converged" G_0W_0 limit. In all cases, we found convergence to be most rapid, if the core-valence interaction was treated on the HF level. For Si, it is sufficient to treat the 3*s* and 3*p* shell as valence, whereas for GaAs, the Ga 3*d* electrons must be included in the valence, and finally for CdS even the 4*p* electrons need to be treated as valence electrons.

Our final calculated G_0W_0 QP energies are, with respect to the top of the valence band, 1.16 eV at X_{1c} for Si, 1.26 eV at Γ_{15c}, 1.51 eV at L_{1c}, and 1.72 eV at X_{1c} for GaAs, and 1.81 at Γ_{1c} for CdS. Overall these values are in between previous all-electron pseudopotential calculations of Tiago *et al.*[6] and the FP-LMTO calculations of Kotani *et al.*[16] The Si QP gap X_{1c}, however, stands out, since our present values are clearly larger than those obtained by the FP-LMTO method (0.98 eV).[44] In this particular case, the present value is supported by recent FLAPW *GW* calculations of Friedrich, who augmented the usual FLAPW basis sets by higher energy derivatives of the one-center wave functions.[42] It is also clear that the present values are systematically smaller than the experimental gaps, reinforcing the argument that a treatment beyond G_0W_0 is required to obtain very accurate QP energies.

ACKNOWLEDGMENTS

This work has been supported by the Austrian *Fonds zur Förderung der wissenschaftlichen Forschung* within the START project. The authors are indebted to F. Bechstedt, L. Reining, and P. Rinke for helpful discussions.

APPENDIX A: NUMERICAL INTEGRATION

To perform the numerical Hilbert transform of the polarizability [Eq. (18)] we evaluate the following frequency dependent weights:

$$t_{ji} = t(\omega_j, \omega_i) = \int_0^\infty d\omega' \Phi_i(\omega') \left(\frac{1}{\omega_j - \omega' - i\eta} - \frac{1}{\omega_j + \omega' + i\eta} \right), \tag{A1}$$

where we introduce triangular shaped functions or finite elements $\Phi_i(\omega')$, centered at frequency ω_i, as

$$\Phi_i(\omega') = \begin{cases} \dfrac{\omega' - \omega_{i-1}}{\omega_i - \omega_{i-1}} & \text{for } \omega_{i-1} \leqslant \omega' \leqslant \omega_i, \\ \dfrac{\omega_{i+1} - \omega'}{\omega_{i+1} - \omega_i} & \text{for } \omega_i \leqslant \omega' \leqslant \omega_{i+1}, \\ 0 & \text{elsewhere.} \end{cases}$$

Here ω' is a continuous variable, whereas ω_i are discrete grid points. The integrals (A1) can be performed analytically. Hilbert transforms such as the one in Eq. (18) can then be performed by a simple summation

$$\chi^0_{\mathbf{q}}(\mathbf{G}, \mathbf{G}', \omega_j) = \sum_i t_{ji} \chi^S_{\mathbf{q}}(\mathbf{G}, \mathbf{G}', \omega_i). \tag{A2}$$

The summation can be done using BLAS3 routines, achieving peak performance on any modern computer platform. It should be noted, that slightly different frequency-dependent weights [Eq. (A1)] must be used for the Hilbert transform of the self-energy [Eq. (10)].

APPENDIX B: FREQUENCY GRID

The discrete frequency grid is chosen recognizing the character of the integrated function. It is prudent to choose a denser grid in the interval where the function changes rapidly and a coarser grid where the function is relatively monotonic. In our case, the integrated function behaving roughly like

$$F(\omega) \approx \frac{1}{\omega^2 - \omega_p^2 \pm i\eta}, \tag{B1}$$

with poles at ω_p. Integrals of the general form

$$I = \int F(\omega) d\omega = \int \frac{F(\omega)}{g(\omega)} g(\omega) d\omega \tag{B2}$$

are most efficiently evaluated by introducing a weighting function $g(\omega)$ and performing a variable substitution $d\nu = g(\omega) d\omega$. We have chosen the following weighting function, which observes the correct asymptotic behavior and is free of a singularity in the interval $[0, \infty[$:

$$g(\omega) = \frac{1 + (\omega/\omega_m)^2}{1 + (\omega/\omega_m)^4}. \tag{B3}$$

The function is one at $\omega = 0$, increases slightly, falls back to one at $\omega = \omega_m$, and finally decays quadratically. The frequency ω_m is adjusted to be at the outermost node of the head of the frequency-dependent microscopic dielectric function or at the position of the bottom of the conduction band with respect to the bottom of the valence band (whichever value is larger). An equally spaced mesh on ν maps onto a nonlinear mesh in ω, where the following relationship is observed:

$$\omega_i = G^{-1}(\nu_i) \quad \text{with } G(\omega') = \int_0^{\omega'} g(\omega) d\omega. \tag{B4}$$

The integral (B2) can then be numerically evaluated as

$$I = \int \frac{F[G^{-1}(\nu)]}{g[G^{-1}(\nu)]} d\nu = \sum_i w_i \frac{F[G^{-1}(\nu_i)]}{g[G^{-1}(\nu_i)]}, \tag{B5}$$

where w_i are weights chosen according to a standard integration scheme (trapezoidal, Simpson, etc.). At present we however only choose a nonequally spaced grid according to Eq. (B4), and then integrate using the finite element basis set (A1) and (A2). We expect that a variable substitution in (A1) would give more accurate results for coarser grids, but this approach has not yet been implemented.

[1] F. Aryasetiawan and O. Gunnarsson, Rep. Prog. Phys. **61**, 237 (1998).
[2] W. G. Aulbur, L. Jonsson, and J. W. Wilkins, Solid State Phys. **54**, 1 (2000).
[3] L. Hedin, Phys. Rev. **139**, A796 (1965).
[4] M. S. Hybertsen and S. G. Louie, Phys. Rev. B **34**, 5390 (1986).
[5] G. E. Engel and B. Farid, Phys. Rev. B **47**, 15931 (1993).
[6] M. L. Tiago, S. Ismail-Beigi, and S. G. Louie, Phys. Rev. B **69**, 125212 (2004).
[7] R. W. Godby, M. Schlüter, and L. J. Sham, Phys. Rev. B **37**, 10159 (1988).
[8] H. N. Rojas, R. W. Godby, and R. J. Needs, Phys. Rev. Lett. **74**, 1827 (1995).
[9] M. M. Rieger, L. Steinberg, I. D. White, H. J. Rojas, and R. W. Godby, Comput. Phys. Commun. **117**, 211 (1999).
[10] L. Steinberg, A. Rubio, L. Reining, M. Torrent, I. D. White, and R. W. Godby, Comput. Phys. Commun. **125**, 105 (2000).
[11] T. Miyake and F. Aryasetiawan, Phys. Rev. B **61**, 7172 (2000).
[12] F. Aryasetiawan and O. Gunnarsson, Phys. Rev. Lett. **74**, 3221 (1995).
[13] M. Rohlfing, P. Krüger, and J. Pollmann, Phys. Rev. B **48**, 17791 (1993).

[14] M. Rohlfing, P. Krüger, and J. Pollmann, Phys. Rev. B **52**, 1905 (1995).
[15] M. Rohlfing, P. Krüger, and J. Pollmann, Phys. Rev. Lett. **75**, 3489 (1995).
[16] T. Kotani and M. van Schilfgaarde, Solid State Commun. **121**, 461 (2002).
[17] F. Aryasetiawan and O. Gunnarsson, Phys. Rev. B **49**, 7219 (1994).
[18] M. Usuda, N. Hamada, T. Kotani, and M. van Schilfgaarde, Phys. Rev. B **66**, 125101 (2002).
[19] P. E. Blöchl, Phys. Rev. B **50**, 17953 (1994).
[20] B. Arnaud and M. Alouani, Phys. Rev. B **62**, 4464 (2000).
[21] S. Lebègue, B. Arnaud, M. Alouani, and P. E. Bloechl, Phys. Rev. B **67**, 155208 (2003).
[22] J. Furthmüller, G. Cappellini, H. C. Weissker, and F. Bechstedt, Phys. Rev. B **66**, 045110 (2002).
[23] N. Hamada, M. Hwang, and A. J. Freeman, Phys. Rev. B **41**, 3620 (1990).
[24] R. Del Sole, L. Reining, and R. W. Godby, Phys. Rev. B **49**, 8024 (1994).
[25] A. Fleszar and W. Hanke, Phys. Rev. B **71**, 045207 (2005).
[26] F. Bruneval, F. Sottile, V. Olevano, R. Del Sole, and L. Reining, Phys. Rev. Lett. **94**, 186402-1 (2005).
[27] W. D. Schöne and A. G. Eguiluz, Phys. Rev. Lett. **81**, 1662 (1998).
[28] B. Holm and U. von Barth, Phys. Rev. B **57**, 2108 (1998).
[29] M. Gajdoš, K. Hummer, G. Kresse, J. Furthmüller, and F. Bechstedt, Phys. Rev. B **73**, 045112 (2006).
[30] J. Paier, R. Hirschl, M. Marsmann, and G. Kresse, J. Chem. Phys. **122**, 234102 (2005).
[31] G. Kresse and D. Joubert, Phys. Rev. B **59**, 1758 (1999).
[32] L. Reining, G. Onida, and R. W. Godby, Phys. Rev. B **56**, R4301 (1997).
[33] E. L. Shirley, X. Zhu, and S. G. Louie, Phys. Rev. B **56**, 6648 (1997).
[34] *Numerical Data and Functional Relationships in Science and Technology*, edited by K. H. Hellwege and O. Madelung, Landolt-Börnstein, New Series, Group III, Vol. 17, part a and Vol. 22, part a (Springer, Berlin, 1982).
[35] W. Ku and A. G. Eguiluz, Phys. Rev. Lett. **89**, 126401 (2002).
[36] *Landolt-Börnstein, Numerical Data and Functional Relationships in Science and Technology*, edited by K. H. Hellwege, O. Madelung, M. Schulz, and H. Weiss, New Series Vol. III, Part 22a (Springer-Verlag, New York, 1987).
[37] L. Ley, R. A. Pollak, F. R. McFeely, S. P. Kowalczyk, and D. A. Shirley, Phys. Rev. B **9**, 600 (1974).
[38] *Semiconductors: Technology of III-V, II-VI and Non-Tetrahedrally Bonded Compounds*, edited by O. Madelung, Landolt-Börnstein, New Series, Group III, Vol. 17, Pt. d (Springer, Berlin, 1982).
[39] P. Blaha, K. Schwarz, G. K. H. Madsen, D. Kvasnicka, and J. Luitz, WIEN2K, an augmented plane wave local orbitals program for calculating crystal properties, edited by K. Schwarz (TU Wien, Austria, 2001).
[40] S. G. Louie, S. Froyen, and M. L. Cohen, Phys. Rev. B **26**, 1738 (1982).
[41] N. Troullier and J. L. Martins, Phys. Rev. B **43**, 1993 (1991).
[42] C. Friedrich, A. Schindlmayr, S. Blügel, and T. Kotani, Phys. Rev. B (to be published).
[43] S. Massidda, M. Posternak, and A. Baldereschi, Phys. Rev. B **48**, 5058 (1993).
[44] S. V. Faleev, M. van Schilfgaarde, and T. Kotani, Phys. Rev. Lett. **93**, 126406 (2004).